Journal of Advanced Research 44 (2023) 185–199

Contents lists available at ScienceDirect

Journal of Advanced Research

journal homepage: www.elsevier.com/locate/jare

Original Article

Soluble Trem2 is a negative regulator of erythrophagocytosis after intracerebral hemorrhage in a CD36 receptor recycling manner

Hang Zhou [1], Jianru Li [1], Libin Hu [1], Jiahui Yu, Xiongjie Fu, Feng Liang, Feng Yan *, Gao Chen *

Department of Neurosurgery, Second Affiliated Hospital, School of Medicine, Zhejiang University, Jiefang Road88th, Hangzhou 310016, People's Republic of China

HIGHLIGHTS

- Soluble Trem2 delays the microglia/macrophages mediated hematoma resolution after ICH
- Soluble Trem2 modulates erythrophagocytosis in a full-length Trem2 independent pathway.
- Soluble Trem2 inhibits CD36 receptor recycling and exacerbates lysosomal degradation of unrecycled CD36 in microglia/macrophages.

GRAPHICAL ABSTRACT

sTrem2 reshapes the ICH-associated microglia/macrophages impairing erythrophagocytosis and enhancing inflammation via inhibition of Vps35-mediated pro-erythrophagocytic molecular receptor CD36 recycling and lysosomal degradation of unrecycled CD36, causing exacerbation of neuronal loss and neurological dysfunction after ICH.

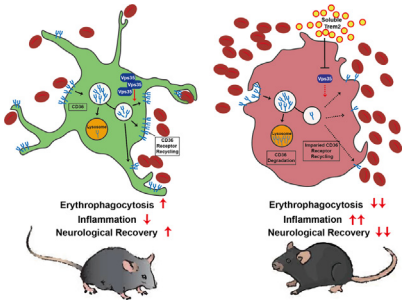

ARTICLE INFO

Article history:
Received 29 November 2021
Revised 23 February 2022
Accepted 15 March 2022
Available online 18 March 2022

Keywords:
Intracerebral hemorrhage
Soluble Trem2
Phagocytosis
Microglia
CD36 receptor recycling

ABSTRACT

Introduction: Microglia and macrophages participate in hematoma clearance after intracerebral hemorrhage (ICH), thereby facilitating tissue restoration and neurological recovery. Triggering receptor expressed on myeloid cells 2 (Trem2) has been indicated as a major pathology-induced immune signaling hub on the microglial/macrophage surface. Soluble Trem2 (sTrem2), the proteolytic form of Trem2, is abundant in the body fluid and is positively correlated with the pathological process.
Objectives: In the present study, we aimed to investigate the potential role of sTrem2 in hematoma resolution after ICH and to elucidate its underlying mechanisms.
Methods: We explored the biological functions of sTrem2 in the murine ICH brain by stereotaxic injection of recombinant sTrem2 protein or by adeno-associated virus-mediated expression. Erythrocyte phagocytosis was assessed using flow cytometry and immunofluorescence. Western blotting was performed to evaluate protein expression. Changes in behavior, sTrem2-induced down-stream pathway, and microglia were examined.
Results: sTrem2 impedes hematoma resolution and impairs functional motor and sensory recovery. Interestingly, sTrem2 bypasses full-length Trem2, negatively regulating microglial/macrophage erythrophagocytosis, and promotes an inflammatory phenotype, which is associated with reduced retromer levels and impaired recycling of the pro-erythrophagocytic receptor CD36. Rescue of retromer Vps35

Peer review under responsibility of Cairo University.

* Corresponding author at: Department of Neurosurgery, Second Affiliated Hospital, School of Medicine, Zhejiang University, Jiefang Road88th, Hangzhou 310016, People's Republic of China.
E-mail addresses: fengyanzju@zju.edu.cn (F. Yan), d-chengao@zju.edu.cn (G. Chen).

[1] H.Z., J.R.L., and L.B.H contributed equally to this work.

https://doi.org/10.1016/j.jare.2022.03.011
2090-1232/

abolishes the phagocytosis-inhibiting effects and lysosome-dependent CD36 degradation caused by sTrem2.

Conclusion: These findings indicate sTrem2 as a negative factor against microglia/macrophage-mediated hematoma and related neuronal damage clearance, provide insight into the mechanisms by which erythrophagocytosis is regulated and how it may be impaired after ICH, and suggest that the anti-proteolytic activity of Trem2 can be explored for ICH therapy.

Introduction

Intracerebral hemorrhage (ICH) is a devastating subtype of stroke that results from blood extravasation within the brain parenchyma [1,2]. The mortality and morbidity of ICH are the highest among all forms of stroke, but we are still lacking a specific therapy [3,4]. The pathological mechanism of ICH involves primary and secondary injury [5]. The extravasated hematoma deforms and compresses the brain tissue, elevating intracranial pressure, which comprises primary injury [6]. Being exposed to blood components, the brain tissue suffers secondary injury resulting from the early activation of the immune system, including microglia, macrophages, and recruited peripheral leukocytes [7]. Secondary injury in ICH is characterized by pro-inflammatory cytokine production, metabolic dysfunction, blood–brain barrier breakdown, oxidative stress, and perihematoma edema, which are detrimental to neuron survival [5].

Hematoma is a key factor that mediates primary and secondary brain damage. The size of the hematoma is an established indicator of ICH severity and a strong predictor of clinical outcome [6]. Recent clinical trials indicated that neither early open nor endoscopic surgery to evacuate hematoma improved functional recovery, compared to medical management of ICH [8-10]. These results demonstrate that mechanical hematoma removal by surgery has limited success in improving ICH outcomes. Therefore, a viable alternative is to boost endogenous pathways for hematoma resolution and red blood cell engulfment to accelerate neurological recovery [11].

Microglia and macrophages are the main immune cells that respond rapidly to acute brain injuries, such as ICH, and play a key role in foreign substance, apoptotic cells, or debris engulfment [12]. The activation and recruitment of microglia and macrophages to the region of bleeding occur several hours after ICH, persistent accumulation in *peri*-hematoma can be observed until weeks after ICH [13-15]. Thus, erythrophagocytosis is a key pathological process in both primary and secondary ICH injuries. Although in hemorrhagic sites the profile and function of microglia and macrophages are diverse and dynamic, enhancement of the phagocytic capability of these phagocytes has been shown to reduce hematoma-induced deleterious mechanical effects, limit neuroinflammation, prevent cytotoxicity, decrease neuronal injury, and improve neurological functions after ICH [13,14]. However, the mechanisms underlying microglial/macrophage phagocytosis remain unclear.

Trem2, a transmembrane receptor, predominantly expressed in microglia and macrophages, and has been recognized as an important regulator of microglial/macrophage functions innate immune, such as phagocytosis, biosynthetic metabolism, proliferation, survival, and cytokine expression [16,17]. Trem2 suffers regulated proteolytic cleavage at the specific peptide region H157–S158 bond, resulting in the shedding of full-length Trem2 then formed as soluble Trem2 (sTrem2). In several neurodegenerative diseases, the concentration of sTrem2 correlates with neuronal injury and pathological progress [18,19]. Recent data indicate that sTrem2 plays a functional role in microglial inflammatory cytokines production and enhanced amyloid-β plaque engulfment [20-22]. However, whether sTrem2 also affects microglia/macrophage regulation and the related phagocytic function in acute brain injury remains to be determined. In this study, we aimed to identify the impacts of sTrem2 in an autologous blood ICH mouse model with two strategies: recombinant sTrem2 protein injection and encoding sTrem2 sequence adenovirus-associated virus (AAV) transfection. Here, we characterize that sTrem2 delayed the resolution of hematoma, exacerbated inflammation, and impaired functional recovery by modulating microglia/macrophage phagocytosis by diminishing the pro-engulfment molecular CD36 receptor recycling. Thus, providing evidence for anti-cleavage of sTrem2 might therefore be worthy of the further clinical translation of ICH.

Material and methods

Ethics statement

All experiments involving animals were conducted according to the ethical policies and procedures approved by the ethics committee of the Second Affiliated Hospital, Zhejiang University, China (Approval no. AIRB-2021–607).

Mice

Sample sizes were adequately powered to observe the effects based on the past experience of animal studies. All the mice used in our experiments were male which housed in home cages with a 12 h light/dark cycle.

For AAV injection, C57BL/6 mice were injected with AAV-Ctrl, AAV-sTrem2, and/or AAV-CD68-Trem2 at 6 weeks of age, when the weight was approximately 20 g. ICH modeling and behavioral tests were performed 4 weeks after AAV injection.

For sTrem2 protein injection, C57BL/6 mice were injected into the right striatum with heat-inactivated sTrem2 or recombined sTrem2 protein mixed with autologous blood. The behavioral tests and samples were harvested for biochemical and histological analyses.

Trem2 $^{-/-}$ mice were established on a C57BL/6 background and purchased from Shanghai Model Organisms Center (#NM-KO-190402, MGI:1913150).

ICH model set up

Autologous blood injection mice ICH models were performed in this study [14]. Briefly, 30 μl autologous blood collected from the tail artery was delivered uniformly within 10 min into the ipsilateral striatum after mice anesthetized by isoflurane. The coordinates for injection were +2.5 mm lateral, and −3.0 mm deep at 5° angle (relative to bregma). The body temperature was maintained at 37.0 °C throughout the procedure by placing the animals on a homeothermic blanket.

AAV delivery

The right striatum of adult mice was injected with 1×10^{11} viral particles (1ul, 1×10^{13} V.G/ml) of AAV2/8-EGFP-T2A-sTrem2-3 × F LAG (AAV-sTrem2) or AAV2/8-EGFP (AAV-Ctrl), which was prepared by Genechem Technology (Shanghai, China).To generate microglia-specific transduction of full-length Trem2, AAV2/9-ZsGreen-CD68-Trem2-MYC or AAV2/9-ZsGreen (AAV-Ctrl) with the microglial specific promoter CD68 which produced by HanBio Technology (Shanghai, China) was injected into the right striatum using 1×10^{11} viral particles 4 weeks before ICH modeling. 10-μL syringe with a 26-G needle (Hamilton, 7642-01, 7803-07) was used in all AAV delivery procedure.

Behavioral tests

All behavioral assessments of each group were performed at similar and relatively fixed time which kept between 7:00 pm and 9:00 pm.

Cylinder test [23]. To observe forelimb paw placement, we placed mice in a transparent plastic cylinder where they were made sure to rear up freely. The first forelimb placed on the wall of the cylinder was scored until reaching 20 rears. Left, right, or both wall touches were recorded. The statistic results were performed as laterality index identified as (right – left) / 20. A higher positive score means a more use of right forelimb and a more severe left hemiparesis.

Corner turn test [1424]. To measure motor and sensory function balance, we proceeded to place mice in a 30° transparent corner where they were allowed to exit the corner via turnning either left or right. The statistic results were calculated as the percentage of right turns in the recorded 10 trials to reflect direction preference.

Forelimb placement tests [14]. To test the innate neurological reflexes of mice, we held the mice body and stimulated their vibrissae by gently brushing them on the edge of a countertop. Each side per mouse was tested 10 times. Control mice could quickly place the ipsilateral forelimb upon vibrissae stimulation, while ICH mice did not respond to vibrissae stimulation. The severity of the injury was calculated as the number of times the mouse suitable forelimb placement out of the total number of trials.

Adult microglia isolation

Mice were sacrificed 1, 3, or 7 days post-ICH modeling after perfusion with isolation medium (HBSS containing 0.05% glucose, 15 mM HEPES, and 0.2% DNase I). Brains were dissected from the mice rapidly, brain slides were cut into 1 mm thickness, and the perihematoma tissues were isolated. Collected tissues were chopped and homogenized in 3 ml of cold isolation medium using a Dounce homogenizer to generate single cells suspension. The suspension was rinsed by another 2 ml medium after filtered through a 100-μm cell strainer. Following 340 × g centrifuge for 5 min, the precipitate was resuspended in 30% Percoll and centrifuged at 900 × g for 20 min with lowest lifting speed to remove myelin [25]. To further purify microglia, precipitated cells were resuspended in MACS buffer and wash twice, then 10 μl of CD11b MicroBeads (Miltenyi Biotec) was added per sample and incubated for 15 min in room temperature. After resuspension, cells were transferred into an LS separation column which placed in a magnetic holder (Miltenyi Biotec) and labeled cells remained in the magnetic field. To gain the CD11b positive cells, carefully removed column from the magnetic field and washed the column with MACS buffer into collection tubes.

Primary microglia culture

For microglial culture [19], brains were dissected from P0–P1 C57BL/6 mice, cortices were isolated, and the meninges were removed in cold HBSS and then dissociated with 0.25% trypsin. The cell suspension was plated onto poly d-lysine-coated T75 cell culture flasks and grown in DMEM containing 10% fetal bovine serum (FBS). The medium added in 25 ng/ml GM-CSF to promote microglial proliferation after 7 days. Primary microglia were harvested by shaking flasks after 2 weeks in culture, then transferred to coverslips or dishes without coating, and sustained in 3% FBS supplemented DMEM for 6–8 h before experiments.

Lentiviral delivery

Microglial cell line BV2 cells were cultured in high-glucose DMEM supplemented with 10% FBS. Lentivirus (LV) containing Vps35, Trem2 or backbone plasmids, which were purchased from Vigene Biosciences (Shandong, China) were transduced. BV2 cells were infected in suitable plates or dishes under 10 mg/ml polybrene added virus-containing media at a multiplicity of infection of 300. Twenty-four hours after infection, cells were refreshed and selected in 2 μg/ml puromycin for 3 days [26]. When lentiviral constructs were well tolerated, cells were transferred to T25 flasks for further experiments, and successful transduction was confirmed by western blotting.

Residual hematoma volume measurement

Mice were sacrificed on day 3 or 7 after ICH. 1-mm-thick coronal sections across the hematoma region were organized after transcardial perfusion with cold PBS according to the established procedure [13,14]. A set of digital images was acquired and analyzed with ImageJ software (NIH) to quantify the residual hematoma volume. After converting the image to 8 bits and inverting it, the area of residual hematoma volume was measured, and the difference in gray value between the hematoma and contralateral regions was calculated. The total residual hematoma volume from these sections was then integrated using the following formula:

$$V = \sum (\text{Areas of hematoma} \times 1)$$

where V is the residual hematoma volume calculated in cubic millimeters. Similarly, the hematoma index was integrated by adding the difference in the gray value. In part of residual hemoglobin content measurement, the brain tissue containing blood from all coronal brain slices were collected and homogenized in 200 μl double-distilled water. To generate the standard curve 0, 0.5, 1.0, 2.0, 4.0, and 8.0 μl whole blood were mixed into normal brain sample then harvested homogenized supernatant after centrifugation at 12,000*g* for 30 min. The aliquot of lysate were picked (20 μl) and incubated in Drabkin's reagent (Sigma-Aldrich) (80 μl) for 15 min. The cyanomethemoglobin level was tested at a wavelength of 540 nm and the corresponding volume was further calculated via standard curve.

mRNA analysis

Total RNA was isolated from cells or tissues using the RNeasy Kit (QIAGEN) according to the manufacturer's instructions. The cDNA was generated by using the PrimeScript™ II 1st Strand cDNA Synthesis Kit (Takara). Applied Biosystems 7500 Real-Time PCR System and One Step TB Green® PrimeScript™ RT-PCR Kit (Takara) were used for next real-time PCR procedure. The primes of PCR were attached in supplementary Table 1. The relative mRNA levels

were normalized to actin based on Ct values, allowing for further comparison.

Fluorescence labeling erythrocytes induction

Red blood cells (RBCs) were isolated from whole murine blood using Ficoll (Sigma-Aldrich) gradient centrifugation, and then washed twice with PBS. The cell membrane fluorescent labeling probe PKH-26 Red Fluorescent Cell Linker Kit (Sigma-Aldrich) or CellTracker CM-DiI Dye (Invitrogen) was used to produce fluorescent erythrocytes [14,23]. To mimic erythrocyte apoptosis, the labeled RBCs were incubated at 56° C for 5 min.

In vivo erythrophagocytosis

The fluorescence–labeled RBCs were suspended by the same donor mice derived plasma with 1:4 ratio as described previously. Then, 30 μl of recombined fluorescent blood was injected into the brains of pretreated mice as same as the autologous blood injection ICH mice model [23,24]. The in vivo erythrophagocytosis in the perihematomal region was analyzed by flow cytometry after 1 or 3 days post-ICH modeling. The LIVE/DEAD^{-}CD45$^{int/hi}$CD11b^{+}-PKH26^{+} population was defined as erythrophagocytic microglia/macrophages.

In vitro erythrophagocytosis

Primary microglia or BV2 cells (3×10^5) were plated on 12-well plate with coverslips. The microglia were then co-cultured with fluorescently labeled apoptotic erythrocytes (5–10 times of phagocytes) at 37° C for 2 h [14]. Extracellular erythrocytes were removed using RBC Lysis Buffer (eBioscience), washed three times with PBS, fixed, and mounted with DAPI and Lectin (FL-1201, Vector Laboratories) on a glass slide. Erythrophagocytosis was observed using a confocal microscope FV3000 (Olympus). The phagocytosis index was performed as the MFI of fluorescent erythrocytes per microglia and showed as the relative change in control groups. For living cell image, the primary microglia were labeled by Lectin for 30 min, 37.0 °C. Then the fluorescence–labeled RBCs were added into culture system, After one hour of RBC settling, the culture dishes were placed into the living cell workstation (Leica, DMi8). images collected at 10-minute intervals and recorded the engulfed cell count for a total of 2 h.

Receptor recycling analysis

Cells were plated on PDL-coated chamber slides at 50–60% confluence. Cells were blocked with 10% donkey serum in DMEM for 15 min, and primary antibodies targeting CD36 (1:100, ab23680, Abcam) were incubated with cells for 1 h at a dilution of 1:100. After acid wash (DMEM, pH 2.0), cells were re-blocked for another 1 h. To label recycled receptors, Alexa Fluor 594-conjugated anti-mouse secondary antibody were used to incubate cells for 1 h. Subsequently, the cells were acid-washed, and fix by 4% PFA. Nuclei labeled by DAPI. Finally, fluorescent signals of recycled receptors or internalized receptors were readily measured by flow cytometry or fluorescence microscopy. According to well-established methods[27,28], quantification of CD36 receptor recycling was calculated by the sum area of fluorescent signals divided by the total cell amount after fluorescent microscopy or the mean fluorescent identity per cell in flow cytometry analysis.

Western blot

Immunoblotting was performed according to standard procedures [29]. Briefly, the tissues and cells were lysed in ice-cold RIPA buffer supplemented with phosphatase and protease inhibitors (Roche) for 30 min. After centrifugation, protein samples with equal amounts of protein were separated by sodium dodecyl sulfate–polyacrylamide gel electrophoresis (SDS-PAGE). After transferring onto polyvinylidene difluoride membranes under constant current of 300 mV for 90 min condition, the membranes were incubated with primary and HRP-conjugated secondary antibodies and visualized using a chemiluminescent reagent. The gray density of the signals on the brands was quantified using the ImageJ software (NIH).

Lysosome isolation

Lysosome enrichment of microglia was extracted using a continuous Percoll-density gradient according to the established protocol [30]. In brief, cells in T75 flasks were collected, washed, and resuspended in ice-cold pH 7.4 sucrose buffer (distilled water containing 250 mM sucrose, 10 mM HEPES, and 1 mM EDTA). The plunge was pulled backward maximally and released eight times after drawing the cell suspension into the chamber of a 10 ml syringe to lyse the cells. Next, 13 ml 18% Percoll diluented by sucrose buffer was slowly delivered by a long catheter, so that it formed a layer below the cell lysate into the ultracentrifuge tube. After ultracentrifugation at 30,000g for 1 h at 4° C, fractions #15–16 (1 ml/fraction) from the top-most layer of the gradient were collected and stored at −80° C, and the cytoplasm and lysosome fractions were analyzed using western blotting.

Results

sTrem2 reduces hematoma resolution and exacerbates neurological dysfunction

To assess the impact of sTrem2 on the process of ICH hematoma resolution, we developed a dedicated mouse model, where we delivered a mixture of recombinant sTrem2 protein and atrial blood into the striatum, causing abundant extracellular sTrem2 in autologous blood. For control mice, we injected heat-inactivated sTrem2 protein and blood mixture as a vehicle (Fig. 1A). Three days after ICH modeling, sTrem2 dramatically elevated the residual hematoma and hemoglobin levels compared to the inactivated form (Fig. 1B). After 7 days, while blood was mostly invisible in the autologous blood injection model [14], the sTrem2 administration enlarged the remaining RBC and its components compared with the inactivated form (Fig. 1C), indicating that high levels of sTrem2 markedly delayed hematoma clearance.

To validate the results from recombinant protein and to further investigate the endogenous impact of high-level sTrem2 on hematoma removal, we generated a murine model by stereotaxic encoding sTrem2 AAV delivery into the right striatum and AAV backbone carrying EGFP cDNA alone as control condition (Fig. 1D). Four weeks after virus delivery, we validated the levels of sTrem2 in the striatum significantly increased compared to control virus infection (Supplementary Fig. 1A, B). On the basis of this animal model, we observed that AAV-sTrem2 significantly increased the hematoma burden both 3 and 7 days post-ICH relative to AAV-Ctrl (Fig. 1E, F), which was consistent with findings from recombinant sTrem2 protein. Next, we evaluated how sTrem2 induced delayed hematoma resolution and affected functional outcomes. Beginning on day 3, abundant sTrem2 led to worse performance on following neurological behavior tests: cylinder (Fig. 1G), corner tests (Fig. 1H) and forelimb placement (Fig. 1I). Seven days post-ICH test performance was still poor, except for corner tests, indicating that sTrem2 contributes to acute disability induced by bleeding. The effects of AAV-mediated overexpression of sTrem2

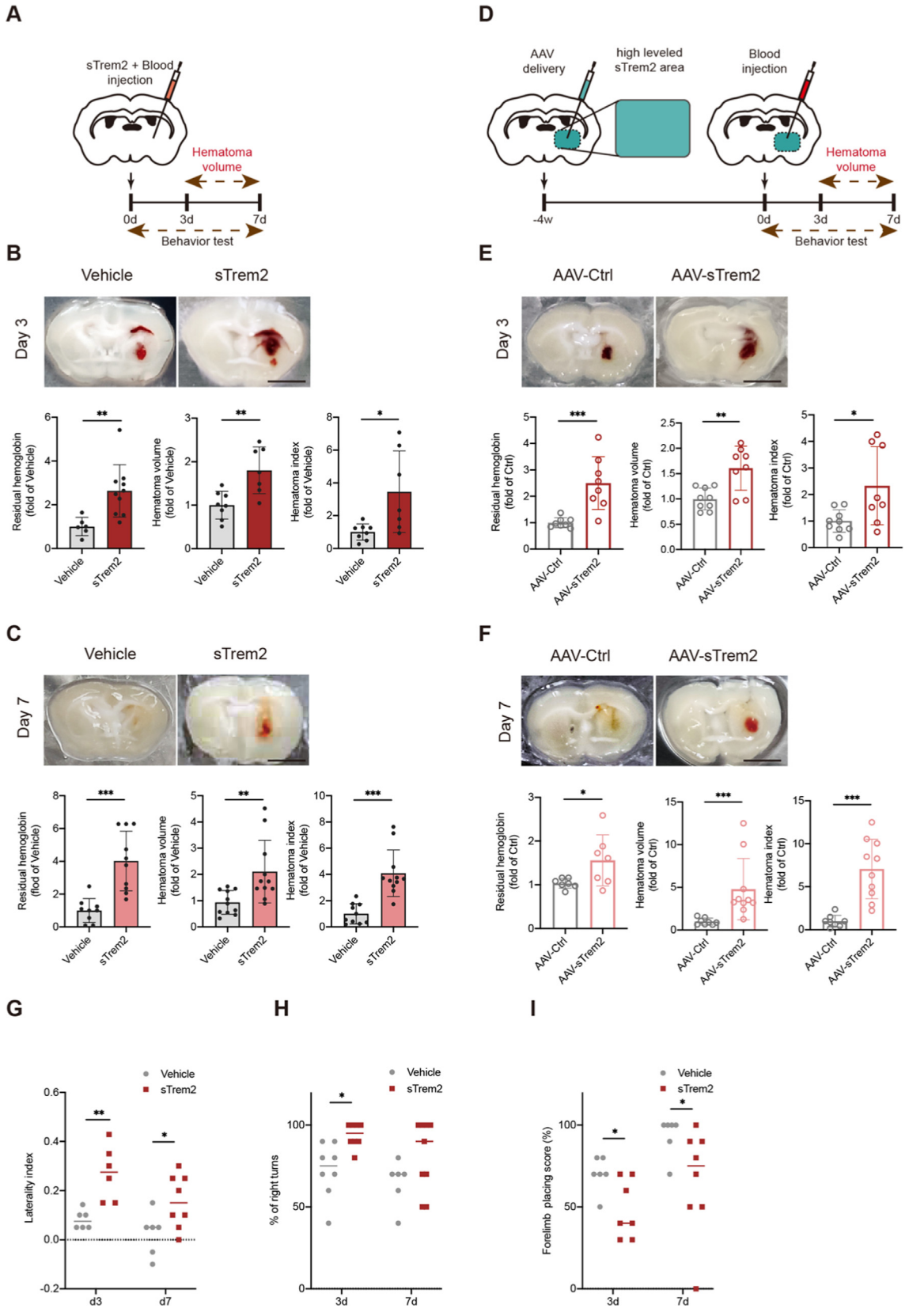
A
sTrem2 + Blood injection
Hematoma volume
0d
3d
7d
Behavior test
D
AAV delivery
high leveled sTrem2 area
Blood injection
Hematoma volume
-4w
0d
3d
7d
Behavior test
B
Vehicle
sTrem2
Day 3
Residual hemoglobin (fold of Vehicle)
Hematoma volume (fold of Vehicle)
Hematoma index (fold of Vehicle)
E
AAV-Ctrl
AAV-sTrem2
Day 3
Residual hemoglobin (fold of Ctrl)
Hematoma volume (fold of Ctrl)
Hematoma index (fold of Ctrl)
C
Vehicle
sTrem2
Day 7
Residual hemoglobin (flod of Vehicle)
Hematoma volume (fold of Vehicle)
Hematoma index (fold of Vehicle)
F
AAV-Ctrl
AAV-sTrem2
Day 7
Residual hemoglobin (fold of Ctrl)
Hematoma volume (fold of Ctrl)
Hematoma index (fold of Ctrl)
G
Vehicle
sTrem2
Laterality index
d3
d7
H
Vehicle
sTrem2
% of right turns
3d
7d
I
Vehicle
sTrem2
Forelimb placing score (%)
3d
7d

were similar to those of recombinant protein-induced neurological dysfunction for the initial 3 days (Supplementary Fig. 1C). Collectively, these results reveal that high levels of sTrem2 impair hematoma clearance, thereby exacerbating neurobehavioral dysfunction.

sTrem2 dampens erythrophagocytosis of microglia/macrophage and neuronal damage recovery

Microglia and macrophages play key role in tissue hemostasis and injury recovery as professional phagocytes by engulfing to clear damaged or harmful cells, such as erythrocytes in the hematoma [13,31]. Thus, we used an in vivo erythrophagocytosis measurement of ICH by injecting autologous RBCs that were fluorescently labeled with a dye prior to injection [14]. Three days post-ICH, $CD45^{int/hi}CD11b^{+}$ microglia/macrophages were identified from striatal single-cell suspensions and by flow cytometry. Quantitative analysis of the erythrophagocytosis number of microglia/-macrophages ($LIVE/DEAD^{-}CD45^{int/hi}CD11b^{+}RBC^{+}$) was significantly reduced in sTrem2 or AAV-sTrem2 injected mice, compared to control mice (Fig. 2A, Supplementary Fig. 2A, C). We used living-cell imaging to determine the in vitro process of microglial erythrophagocytosis. These results suggest that the ability of microglia to phagocytose fluorescently labeled RBCs was impaired in the presence of sTrem2, but not in the presence of heat-inactivated protein (Fig. 2B). We further confirmed this finding by fluorescent microscopy and flow cytometry 2 h after microglia and fluorescent RBC co-culture, according to the results of living-cell imaging. The engulfment of microglia was reduced both in quantity and capability under sTrem2 treatment, compared to inactivated sTrem2 (Fig. 2C), and flow cytometry results indicated that sTrem2 markedly decreased the erythrophagocytic capability of microglia (Fig. 2D), as well as that of microglial cell line BV2 cells [26] (Supplementary Fig. 2B, D), compared with the vehicle group.

Next, we investigated whether the erythrophagocytosis disability of microglia/macrophages induced by sTrem2 exacerbated neuronal injury, which is the cause of ICH-associated behavioral dysfunction [23]. As expected, AAV-sTrem2 delivery significantly enhanced the neuronal loss induced by ICH damage at day 3, as determined by Nissl staining and TUNEL positive signals, compared with AAV control infection (Fig. 2E, F). Collectively, these results reveal that high level of sTrem2 impaired hematoma clearance by disrupting microglia/macrophage-mediated erythrophagocytosis, thereby exacerbating residual hematoma-associated neuronal injury and neurobehavioral dysfunction after ICH.

sTrem2 reshapes microglial response to hematoma

Microglia-derived neuroinflammation has been implicated in the progression of ICH. It has been indicated that diverse microglia morphologies correlate to microglial functions including phagocytosis and inflammatory response [13,23,31]. Here, we tested whether the microglia responses that infiltrated into perihematomal tissues were affected by sTrem2. Firstly, we sketched microglia by Iba1 staining for further morphological analysis (Fig. 3A). In AAV-sTrem2 infected mice, Sholl analysis clearly illustrated that the branching profile of $Iba1^{+}$ cells in the perihematomal region 3 days post-ICH was shifted to the left compared with that in AAV-Ctrl mice (Fig. 3B), indicating decreased branching as a function of distance from the soma, especially at the cellular termini. Furthermore, the area under the curve analysis of $Iba1^{+}$ cell morphology revealed that sTrem2 significantly reduced the volume of microglia/macrophages (Fig. 3C). Finally, we measured the levels of inflammatory cytokines in the microglia/macrophage response to ICH. We isolated ICH-associated phagocytes from perihematomal tissues using CD11b MicroBeads for the next analysis [28] (Fig. 3D). Strikingly, the $CD11b^{+}$ cells sorted from AAV-sTrem2 mice that received autologous blood injection showed a significant upregulation in pro-inflammatory cytokines such as IL-1β and CCL5, which have been associated with worse outcomes in ICH patients (Fig. 3E). Thus, in in vivo models where sTrem2 burden is high and hematomas are present, microglia/microphages shift toward an inflammatory transformation opposed to the pro-phagocytosis phenotype.

sTrem2 modulation of erythrophagocytosis bypasses Trem2 on microglia/macrophages

Trem2 alters the phagocytic capacity of microglia or macrophages to respond to apoptotic cells by recognizing PtdSer [32,33], and engulfment of erythrocytes has been proven to occur through a PtdSer-dependent pathway [14]. However, the role of Trem2 in erythrophagocytosis after ICH remains unknown. Interestingly, significantly more residual hemoglobin and a larger volume of hematoma were observed in the Trem2 KO brain 3 days post-injury (Supplementary Fig. 3A). Next, we evaluated the degree of hematoma resolution between AAV-Trem2 and AAV-Ctrl (CD68-driven AAV backbone carrying Zsgreen cDNA alone) transfected mice (Fig. 4A, Supplementary Fig. 4A, B). As expected, the residual hemoglobin and hematoma volume were significantly decreased in the AAV-Trem2 compared to AAV-Ctrl mice 3 days post-ICH (Fig. 4B). In addition, behavioral analysis performed 3 days after ICH revealed that Trem2 KO mice had worse outcomes compared to WT mice (Supplementary Fig. 3B). The mice with full-length Trem2 microglia-specific transfection showed more rapid recovery in neurobehavioral performance (Fig. 4C). After 7 days, both control and AAV-Trem2 administered mice had similar levels of residual hemoglobin and volume (Supplementary Fig. 4C). Interestingly, when the bleeding was nearly removed in both groups (day 7), AAV-Trem2 mice still had better functional outcomes than control mice (Supplementary Fig. 4D). These data imply that full-length Trem2 in microglia is conducive to hematoma clearance and functional recovery after ICH.

Then, we hypothesized that the upregulation of full-length Trem2 in phagocytes, which promotes erythrophagocytosis, could inhibit sTrem2 negative effects. To test this possibility, we quantified hematoma clearance and behavior in the animal model: autologous blood ICH mice with AAV-sTrem2 and AAV-CD68-Trem2 co-injection and their AAV-Ctrl co-injection, respectively (Fig. 4D). Unexpectedly, the AAV-sTrem2/AAV-CD68-Trem2 co-injected

Fig. 1. sTrem2-induced hematoma deposition inhibits neurological functional recovery after ICH. (A) The C57 mice were injected in the right striatum with vehicle (heat-inactivated sTrem2) or 5 μg of sTrem2 protein, which were mixed with autologous blood to reach the final volume 30 μl. (B, C) Top: Representative coronal sections showing hematoma from Vehicle- (left) and sTrem2- (right) treated mice after blood injection-induced ICH on day 3 and 7, scale bar = 5 mm. Bottom: Quantification of residual hemoglobin, hematoma volume, and hematoma index (volume × density). n = 6–10 per group. $^{*}p < 0.05$, $^{**}p < 0.01$, $^{***}p < 0.001$ versus Vehicle by Student's *t* test. (D) AAV-mediated sTrem2 expression in C57 mice, ICH modeling was established 4 weeks after infection. (E, F) Top: Representative coronal sections showing residual hematoma in AAV-Ctrl (left) and AAV-sTrem2 (right) transfected mice 3 and 7 days post ICH, scale bar = 5 mm. Bottom: Quantification of residual hemoglobin, hematoma volume, and hematoma index. n = 7–9 per group. $^{*}p < 0.05$, $^{**}p < 0.01$, $^{***}p < 0.001$ versus vehicle by Student's *t* test. (G-I) Behavioral test results of cylinder test (G), corner turn (H), and forelimb placement (I) of Vehicle and sTrem2 mice at day 3 and 7 after ICH. n = 6–8 per group. $^{*}p < 0.05$, $^{**}p < 0.01$ by one-way ANOVA and Tukey's post hoc test.

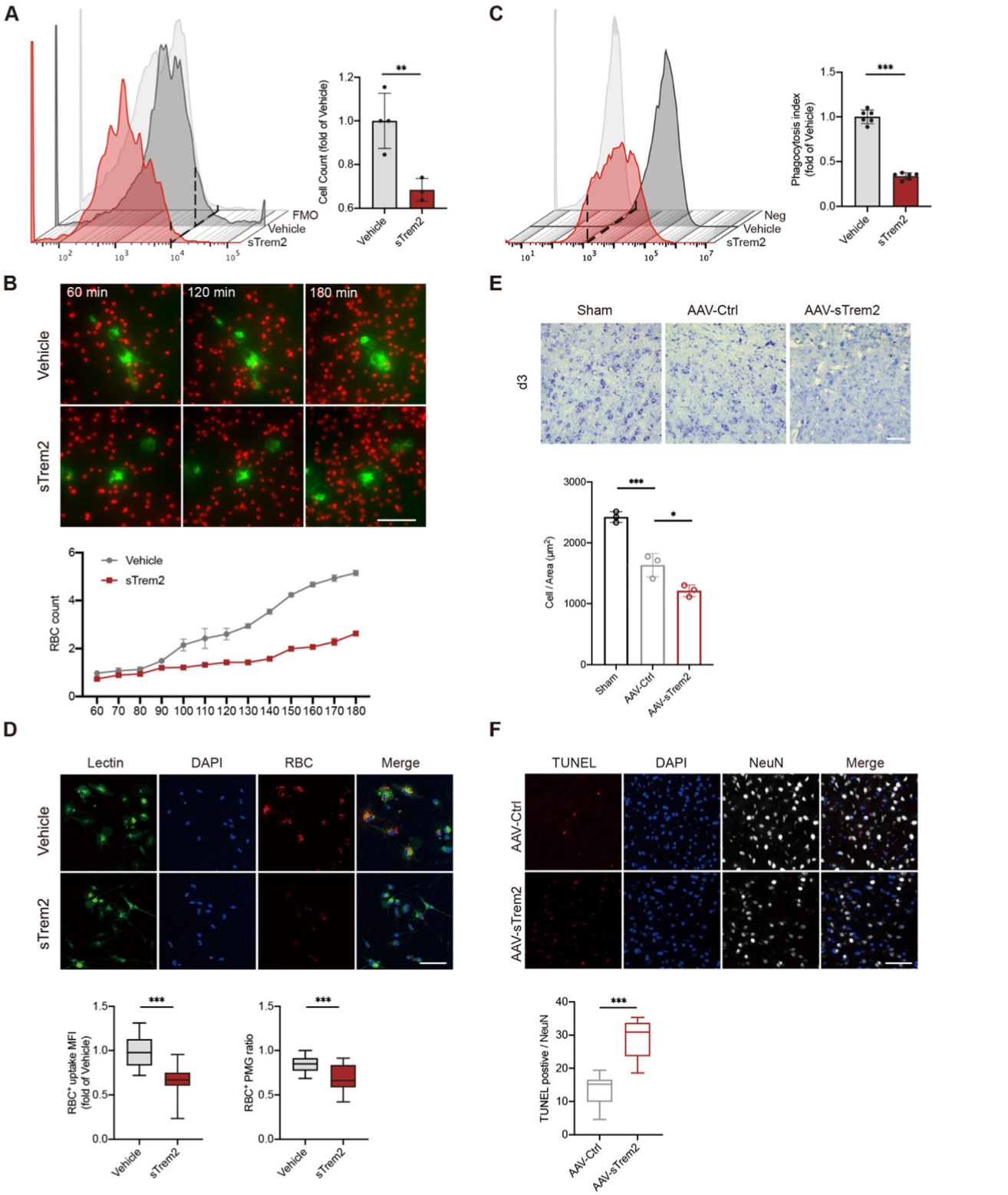

Fig. 2. sTrem2 impairs erythrophagocytosis by microglia/macrophages, which results in more severe neuronal damage after ICH. (A) Flow cytometry histogram showing intensity of fluorescently labeled erythrocytes in microglia/macrophages and quantification of relative change of erythrophagocytes in Vehicle- and sTrem2-treated mice at day 3 after ICH (left). n = 4 per group. **p < 0.01 versus Vehicle by Student's *t* test. (B) Representative images from live-cell imaging (top) at various times after the co-culture of RBC (red) with primary cultured microglia labeled by Lectin (green), scale bar = 20 μm. Monitoring of phagocytosed RBC number over time (bottom). (C) Representative histogram showing primary microglial erythrophagocytosis (left) and quantification of phagocytic index, calculated as intensity of labeled fluorescence in phagocytic microglia. n = 6 per group ***p < 0.001 versus Vehicle by Student's *t* test. (D) Primary microglia were stained with Lectin (green) and DAPI (blue) for nuclei, and with PKH26 for RBC to identify microglia erythrophagocytic phenotype (top). The percentage of phagocytosis and engulfed fluorescent intensity were calculated (bottom). Scale bar = 50 μm, n = 3 per group. **p < 0.01, ***p < 0.001 by Mann–Whitney *U* test. (E) Nissl staining was performed in coronal brain sections from Vehicle- and sTrem2- treated mice 3 days after ICH (top). The number of Nissl body-positive cells was quantified (bottom), scale bar = 50 μm. n = 3 per group, *p < 0.05, ***p < 0.001 by one-way ANOVA and Tukey's post hoc test. (F) TUNEL (red) and NeuN (gray) staining of perihematomal area in coronal brain sections of each group 3 days post ICH (top), and analysis of TUNEL positive cells quantification (bottom). Scale bar = 50 μm, n = 3 per group, **p < 0.01 by Mann–Whitney *U* test.

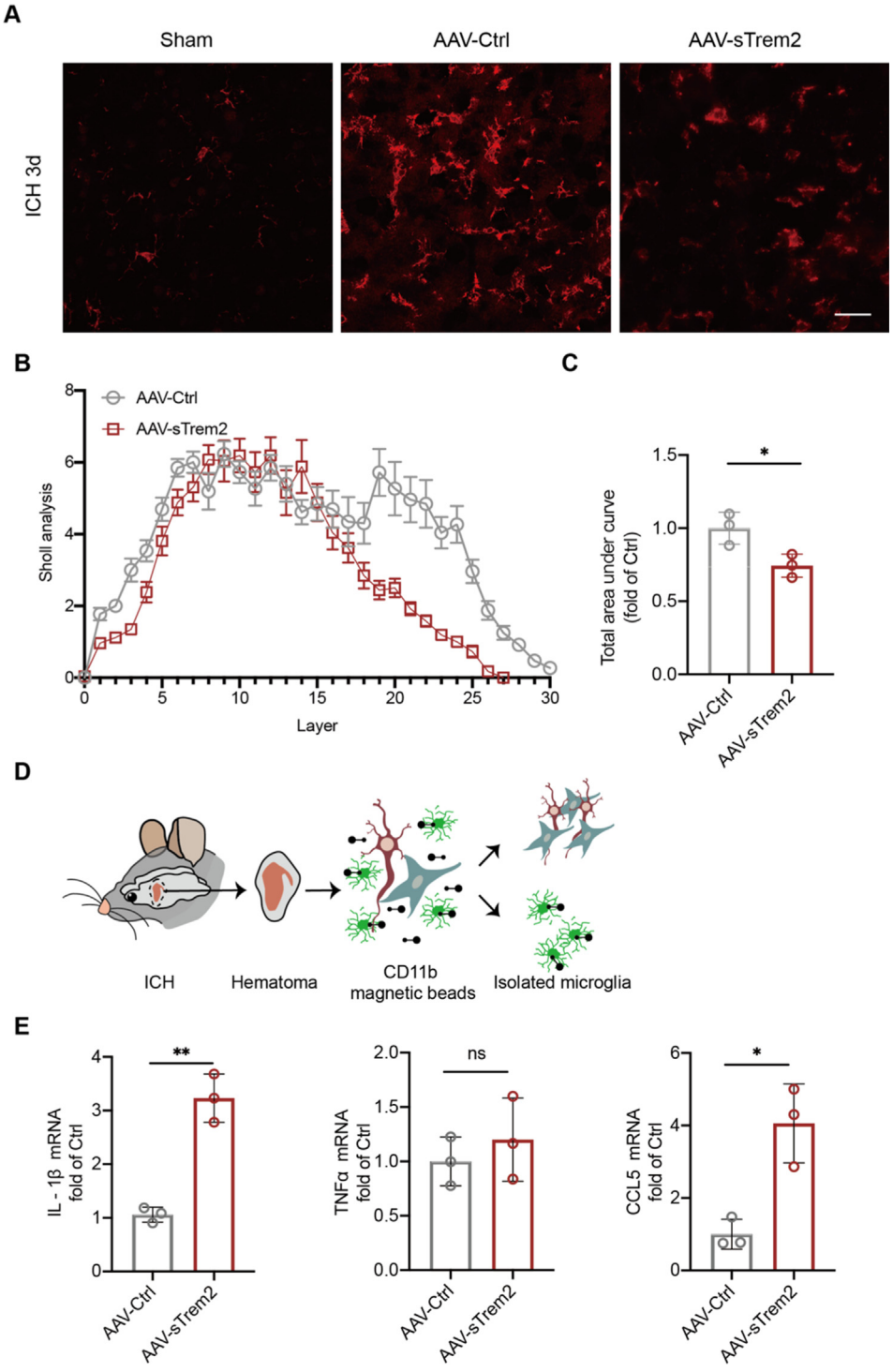

Fig. 3. sTrem2 modulates perihematomal microglial responses of phenotype and inflammation after ICH. (A) Representative brain slices from AAV-Ctrl and AAV-sTrem2-treated mice were stained with anti-Iba1 antibodies to label microglia. Scale bar = 50 μm. (B, C) Quantification of microglial processes by Sholl (left), and the total areas under curve (AUC) analyses (right). n = 3 per group, *p < 0.05 by Student's *t* test. (D) Schematic of the adult microglia in isolated perihematomal area from ICH mice. (E) Quantitative PCR analysis of inflammatory mRNA in isolated microglia from AAV-Ctrl or sTrem2 infected mice 3 days after ICH. n = 3 per group, *p < 0.05, **p < 0.01 by Student's *t* test.

mice presented larger residual hematoma compared with AAV-Ctrl-infected mice (Fig. 4E, Supplementary Fig. 4E) both 3 and 7 days post-ICH, and met comparable levels with AAV-sTrem2 mice. The recovery of neurological functions in the AAV-sTrem2/AAV-CD68-Trem2 co-injected mice was delayed compared to that in control virus-delivered mice but showed similar procedure with AAV-sTrem2 mice (Fig. 4F, Supplementary Fig. 4F). Moreover, quantitative analysis of 3 days of microglial erythrophagocytosis performed in each group revealed a significant enhancement in AAV-CD68-Trem2 infected microglia, while the abundant extracellular sTrem2 abolished the Trem2 mediated phagocytosis (Fig. 4G). In vitro erythrophagocytosis analysis (Fig. 4H) confirmed the in vivo results regarding the effect of sTrem2 on BV2 cells overexpressing Trem2 via lentivirus (Supplementary Fig. 4G). To further validate the relationship between sTrem2 and full-length Trem2, we injected recombinant sTrem2 protein or control protein mixed

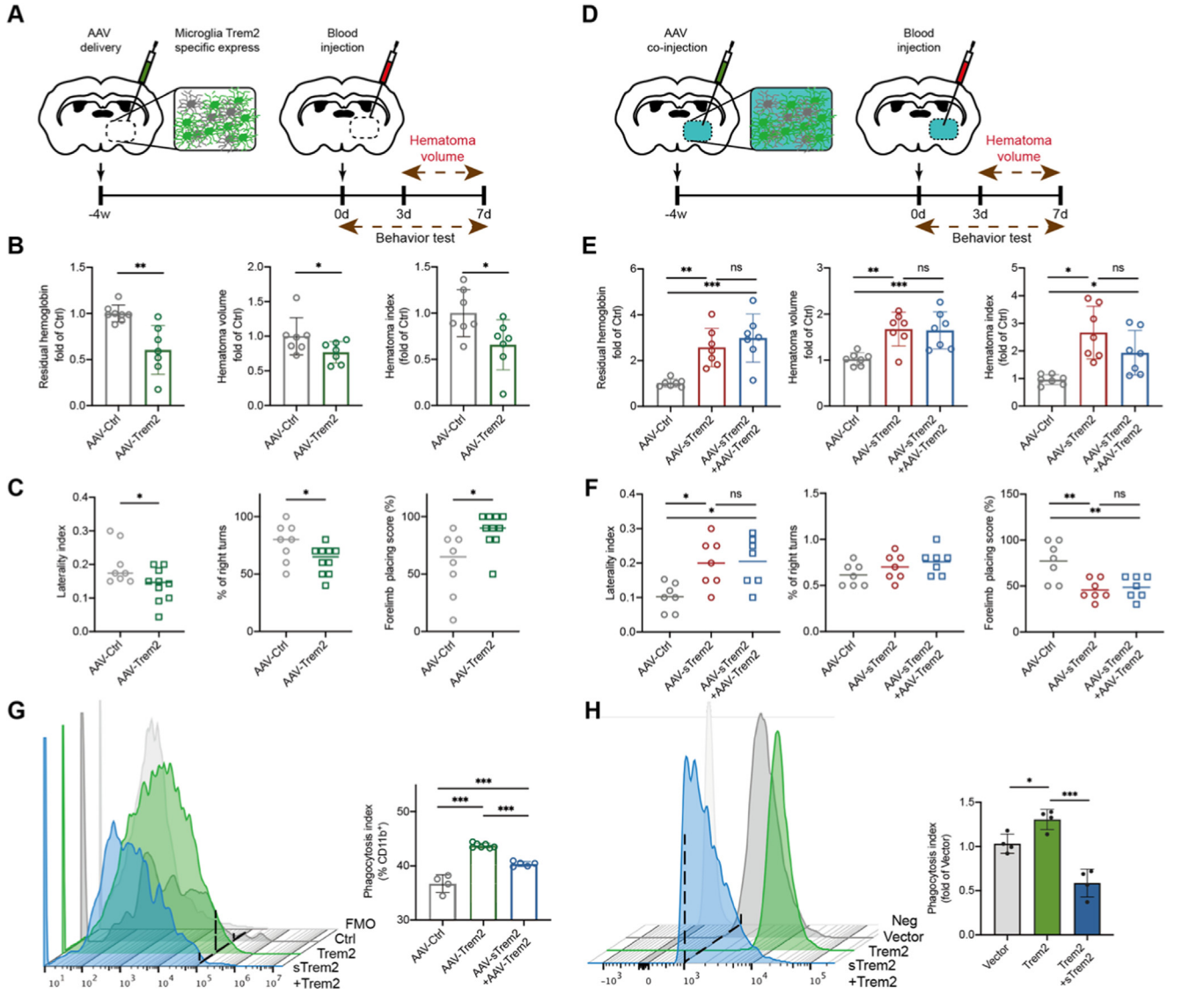

Fig. 4. sTrem2 impedes hematoma resolution independently of full-length Trem2 expressed in microglia. (A) A diagram for the specific transduction of full-length Trem2 by AAV with CD68 promotor in the right striatum of C57 mice. (B) Quantification of residual hemoglobin, hematoma volume, and hematoma index (volume × density) from AAV-CD68-Ctrl and AAV-CD68-Trem2 mice 3 days post ICH. n = 7 per group. *p < 0.05, **p < 0.01 versus AAV-Ctrl by Student's *t* test. (C) Behavioral test results of cylinder test, corner turn, and forelimb placement of AAV-Ctrl and AAV-Trem2 mice 3 days after ICH. n = 7 per group. *p < 0.05 versus AAV-Ctrl by Student's *t* test. (D) A diagram for the mice model of overexpressed full-length Trem2 microglia with high concentration of extracellular sTrem2. (E) Residual hemoglobin, hematoma volume, and hematoma index of AAV-Ctrl, AAV-sTrem2 and AAV-CD68-Trem2 + AAV-sTrem2 -treated mice 3 days post ICH. n = 7 per group. *p < 0.05, **p < 0.01, ***p < 0.001 versus AAV-Ctrl by one-way ANOVA and Tukey's post hoc test. (F) Behavioral tests results of AAV co-injected mice at day 3. n = 7–9 per group, *p < 0.05, **p < 0.01 versus AAV-Ctrl by one-way ANOVA and Tukey's post hoc test. (G) Flow cytometry histogram showing in-vivo erythrophagocytosis in microglia/macrophages and quantification of phagocytic index in each group relative to AAV-Ctrl. N = 4–5 per group, ***p < 0.001 versus AAV-Ctrl by one-way ANOVA and Tukey's post hoc test. (H) In-vitro analysis of BV2 phagocytosis of fluorescent labeled RBC under full-length Trem2 transfection with/without sTrem2 protein stimulation. n = 4 per group, *p < 0.05, ***p < 0.001 versus Vehicle by one-way ANOVA and Tukey's post hoc test.

in blood into Trem2 KO mice. Although Trem2 KO mice showed delayed hematoma resolution, sTrem2 still negatively regulated the clearance process at 3 days post-ICH, which suggested that sTrem2 was independent with full-length Trem2 in erythrophagocytosis (Supplementary Fig. 3C). These findings indicate that sTrem2 can overcome Trem2-induced phagocytic enhancement of microglia both in vivo and in vitro after ICH.

sTrem2 disrupts recycling of erythrophagocytic receptor CD36

Previous studies noticed a gradual increase in the expression of CD36, a scavenger receptor found in microglia and macrophages associated with alternative activation and RBC phagocytosis after ICH [34]. Contrasting the activity of phagocytic promotion receptors, the powerful phagocytosis-inhibiting signal CD47 is expressed in phagocytes, which functions in interaction with its receptor SIRPα [35]. To assess sTrem2 contribution to erythrophagocytic receptors, we evaluated the expression of the two representative markers described above. We found that sTrem2 significantly altered the CD36 level in $CD45^{int/hi}CD11b^{+}$ cells at day 3, but not SIRPα level, compared to control mice brains in two mouse models (Fig. 5A, Supplementary Fig. 5A). We then detected CD36 gene expression in the isolated $CD11b^{+}$ cells, and results showed that sTrem2 did not affect CD36 mRNA levels in phagocytes at day 3 (Supplementary Fig. 5B). We hypothesized that the mRNA might change earlier, thus we detected CD36 gene expression in phagocytes at day 1 as well. However, there were still no changes in the CD36 mRNA levels of

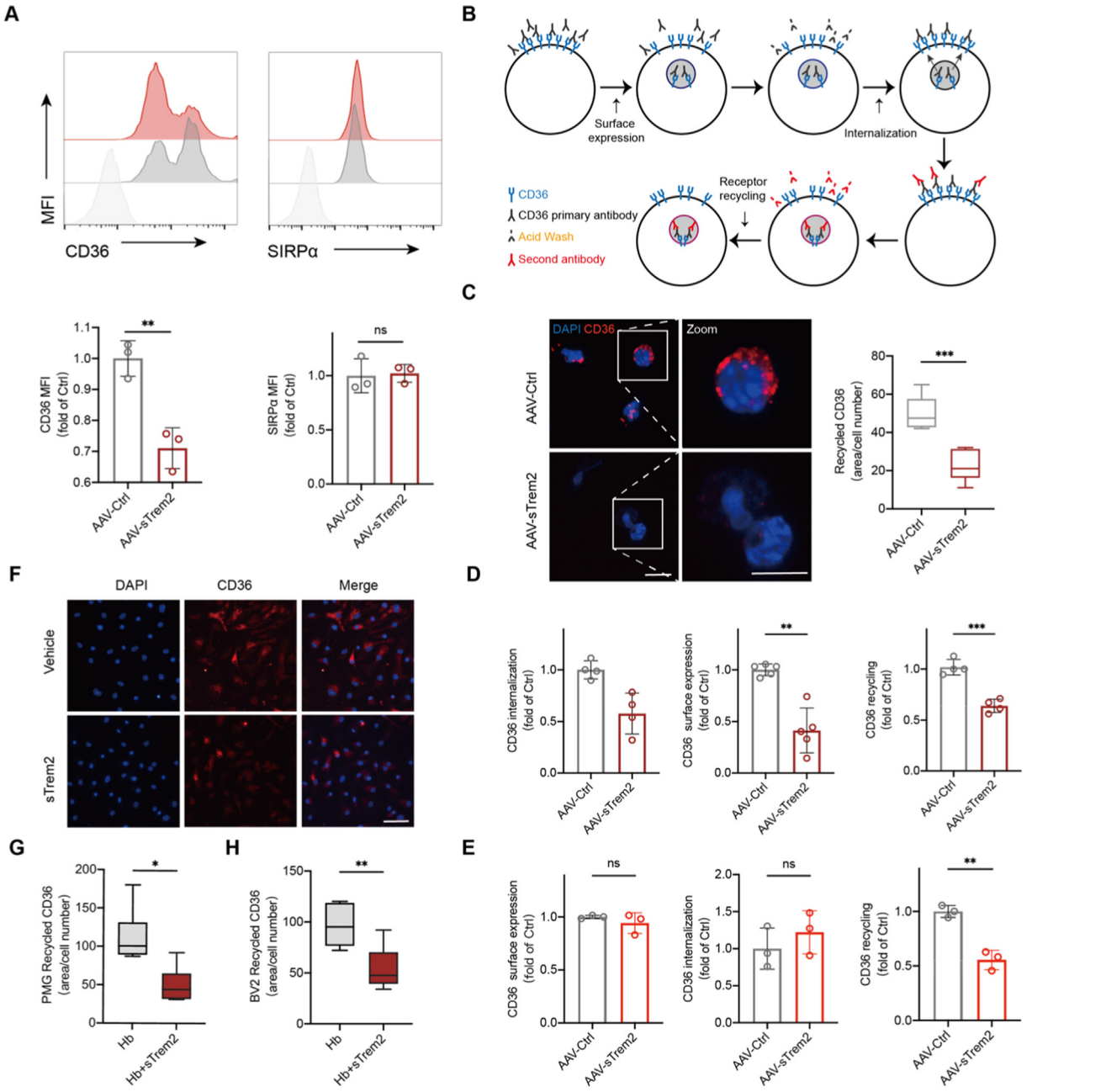

Fig. 5. CD36 receptor recycling is a target of sTrem2 during erythrophagocytosis. (A) Representative histogram displaying the distribution of CD36 and SIRPα in microglia/macrophage treated with AAV-Ctrl or AAV-sTrem2 3 days post ICH (top). Quantification of the mean fluorescence to indicate the cell surface marker change (bottom). n = 3 per group, $^{**}p < 0.01$ versus AAV-Ctrl by Student's *t* test. (B, C) Using an established receptor recycling assay, CD36 receptor recycling was analyzed in magnetic beads isolated cells from AAV-Ctrl and AAV-sTrem2 mice 3 days post ICH. Scale bar = 10 μm. The positive pixels in cells were quantified as recycling CD36. N = 4 per group, $^{***}p < 0.001$ by Mann–Whitney *U* test. (D) $CD11b^+$ cells isolated from AAV-Ctrl or AAV-sTrem2 brains 3 days after ICH were used for surface expression (left), internalization (middle) and recycling (right) of CD36 assay by flow cytometry. N = 5 per group, $^{**}p < 0.01$, $^{***}p < 0.001$ versus AAV-Ctrl by Student's *t* test. (E) Analysis of CD36 surface expression (left), internalization (middle) and recycling (right) in $CD11b^+$ from 1 day post-ICH brains by flow cytometry. n = 3 per group $^{**}p < 0.01$ versus AAV-Ctrl by Student's *t* test. (F) CD36 receptor recycling was analyzed in primary microglia and BV2 under sTrem2 and vehicle treatment (Hb) after hemoglobin stimulation. Scale bar = 50 μm. n = 3 per group, $^{*}p < 0.05$, $^{**}p < 0.01$ versus Hb by Student's *t* test.

microglia/macrophages in the presence of abundant sTrem2 after ICH (Supplementary Fig. 5C).

Accordingly, CD36 is recycled back to the cell surface for reuse upon binding and internalization of substrates, while disruptions in the recycling process have dramatic consequences on phagocytic capability [28,36]. Indeed, $CD11b^+$ cells isolated 3 days post-ICH in AAV-sTrem2 mice showed a prominent reduction in the recycling of the erythrophagocytic receptor CD36 (Fig. 5C). Primary microglia and BV2 cells treated with sTrem2 also showed a similar deficiency in CD36 recycling compared to the vehicle (Fig. 5F-H, Supplementary Fig. 5D). Furthermore, our analysis of cell surface expression and internalization of CD36 in $CD11b^+$ cells isolated 3 days after ICH of AAV-sTrem2 mice showed significantly diminished CD36 recycling in flow cytometry analysis, which was consistent with the above results (Fig. 5D). Interestingly, in the isolated $CD11b^+$ cells from ICH day 1 tissue, sTrem2 disrupted CD36 recycling but had no effect on either CD36 surface expression or internalization (Fig. 5F). Therefore, our data indicate a failure in returning CD36 to the plasma membrane following initial internalization induced by sTrem2, which impaired hematoma clearance.

sTrem2 reduces Vps35 in CD36 receptor recycling

Recycling of CD36 receptors on the cell surface requires the retromer complex, which is responsible for endosome-to-Golgi retrograde sorting and transport of membrane proteins [37]. Several autophagy proteins (Beclin1, Atg5, and Vps34 etc.) regulate the complex [38]. Thus, we sought to understand the mechanism by which sTrem2 impairs CD36 recycling by modulating the retromer complex. To test this, we assessed the impact of sTrem2 on Beclin1 and VPS35 expression. We observed no difference in Beclin1 expression between sTrem2 or control condition in isolated $CD11b^+$ cells from day 3 and day 1 post-ICH (Fig. 6A, B). However, sTrem2 markedly decreased Vps35 expression from day 1 to day 3, and changes in CD36 were consistent with the disruption of CD36 recycling, as reported above (Fig. 6A, B). Primary cultured microglia and BV2 cells also showed a similar decrease in Vps35, but not in Beclin1, under sTrem2 administration (Fig. 6C, Supplementary Fig. 6A). Moreover, we also detected Vps35 levels in $CD11b^+$ cells from AAV-CD68-Trem2 mice after ICH. As expected, the microglial-targeted full-length Trem2 transfection did not affect cellular Vps35 expression. This result indicates that Trem2-induced erythrophagocytosis promotion was abolished by sTrem2-mediated Vps35 decrease (Supplementary Fig. 6B). To further evaluate the role of Vps35 in the sTrem2 modulation pathway, we overexpressed Vps35 in BV2 cells using a lentivirus (Supplementary Fig. 6C), and subsequently investigated whether CD36 recycling was rescued by sTrem2 treatment. Remarkably, Vps35 overexpression resulted in a prominent rescue of CD36 recycling in the presence of sTrem2, while there was no significant change in the baseline condition (Fig. 6D-F). Vps35 restored CD36 recycling against sTrem2, which in turn significantly dampens erythrophagocytosis (Fig. 6G). Therefore, Vps35 facilitates the recycling of CD36 to the plasma membrane while being a potential target of sTrem2, which decreases microglial phagocytosis after ICH.

sTrem2-induced Vps35 deficiency exacerbates CD36 accumulation in lysosomes and degradation

It has been reported that missorted receptors from recycling often lead to lysosomal degradation [39,40]. To further understand the role of sTrem2 in CD36 internalization and recycling via Vps35 blockade, we analyzed the immunofluorescence colocalization of CD36 with Lamp1, a lysosomal marker, in primary microglia and BV2 cells. The sTrem2 treated primary microglia and BV2 cells showed a significant increase in the number of merged puncta, indicating a greater accumulation of lysosomal CD36 compared with vehicle treated cells (Fig. 7A, B). When the receptor recycling blockade was removed via Vps35 rescue, we found less colocalization of CD36 with Lamp1, compared to control sTrem2 treated cells (Fig. 7C, D). In addition, we isolated and purified lysosomes by continuous density gradient centrifugation and found that a higher number of CD36 accumulated in lysosome fractions after sTrem2 treatment compared with vehicle (Fig. 7E, F). To further determine whether the accelerated CD36 degradation caused by Vps35 deficiency is lysosome-associated, we analyzed the lysosomal CD36 content. We found that sTrem2 induced lysosomal CD36 was significantly decreased in Vps35 overexpressed BV2 cells compared to control cells (Fig. 7C, D). In agreement with the in vitro findings, the $CD11b^+$ cells sorted from the 1 day post-ICH brain of AAV-sTrem2 mice showed greater accumulation of CD36 in lysosomes than that from AAV-Ctrl mice (Fig. 7G, H). Therefore, our data indicated that sTrem2 might interact with Vps35, thereby promoting CD36 degradation through the lysosome pathway.

Discussion

In this study, we identified a previously undefined and novel role of sTrem2 in diminishing innate hematoma resolution and neurological recovery, which is independent of full-length Trem2 in murine models of ICH. Specific overexpression of Trem2 in microglia and macrophages markedly enhanced hematoma clearance and neurological performance, whereas AAV or recombined protein delivery of sTrem2 in WT mice or in Trem2 treated mice resulted in increase of the inflammatory phenotype and impaired erythrophagocytosis and tissue protection after ICH. Recycling of CD36, a recognized pro-erythrophagocytic molecule, was suppressed in microglia/macrophages with sTrem2 overexpression after ICH through Vps35 inhibition and lysosomal degradation. Collectively, our data set a conclusion that sTrem2 plays a prominent role in phagocytes, through which it can hamper the histological and neurofunctional recovery after ICH.

Microglia show dynamic changes in phenotype after ICH, switching to a pro-inflammatory phenotype in the early phase after ICH (day 1 - day 3) before transitioning to a phenotype associated with recovery (day 3 – day 28) [13,41]. On day 3 after ICH, the transcriptional profile of microglia is closest to the naive state, which suggests that at this time point two microglial phenotypes coexist, indicating an impasse in microglial transformation [13]. Moreover, the rapid infiltration and accumulation of peripheral monocytes derived macrophages were observed at 3 days after ICH [14]. Microglia and macrophages are the main scavenger cells that lead to hematoma clearance by erythrophagocytosis, which temporally and spatially confines neurotoxic RBCs and RBC-derived products, thereby limiting secondary brain damage induced by ICH [23]. In our study, we established correlations between volume of residual hematoma and neurobehavior dysfunction in different cohorts of autologous ICH animals with different interventions (AAV or recombinant protein delivery), strongly supporting the centrality of microglia/macrophage-mediated hematoma resolution in the functional recovery process after ICH. In addition, accumulating evidence indicated that engulfment of eryptotic erythrocytes could not only induce phagocyte reparative phenotype, but also influence surrounding cells in the tissue microenvironment toward anti-inflammatory polarization via lactate and other cytokines release, such as TGFβ and IL-10 [42-44]. We found that erythrophagocytosis impaired microglia/macro phage-reinforced pro-inflammatory characteristics, such as overactivated, amoeboid-shaped cell bodies with spheroid swelling, as well as the transcriptional upregulation of pro-inflammatory genes (IL-1β, and CCL5). Although our results set up the interaction between microglial inflammatory response and erythrophagocytosis function consistent with previous study [14], we still noticed not all proinflammation cytokines were affected (like Tnfα). The time course to detection might be a possible aspect [13,14], however, the detailed mechanisms of different changes among inflammatory cytokines remain further elusive. The contribution of monocyte-derived macrophages mediated phagocytosis to hematoma resolution and the underlying mechanisms which may be different with microglia after ICH require further investigation. Thus, modulating phagocytosis and its associated processes in microglia and macrophages should be explored as potential therapeutic strategy for hemorrhagic stroke.

Recent studies have unraveled the varietal roles of Trem2 in microglia functional modulation in metabolism, survival, phagocytosis, and immune response [45-48]. The loss of Trem2 results in reduced phagocytosis, while increased Trem2 gene dosage enhances phagocytic activity and limits β-amyloid-mediated spread of pathogenic tau [48]. The Trem2 positive microglia also play a key role in oxidized phosphatidylcholines promotion, degenerated myelin clearance, synapse formation, and lipid

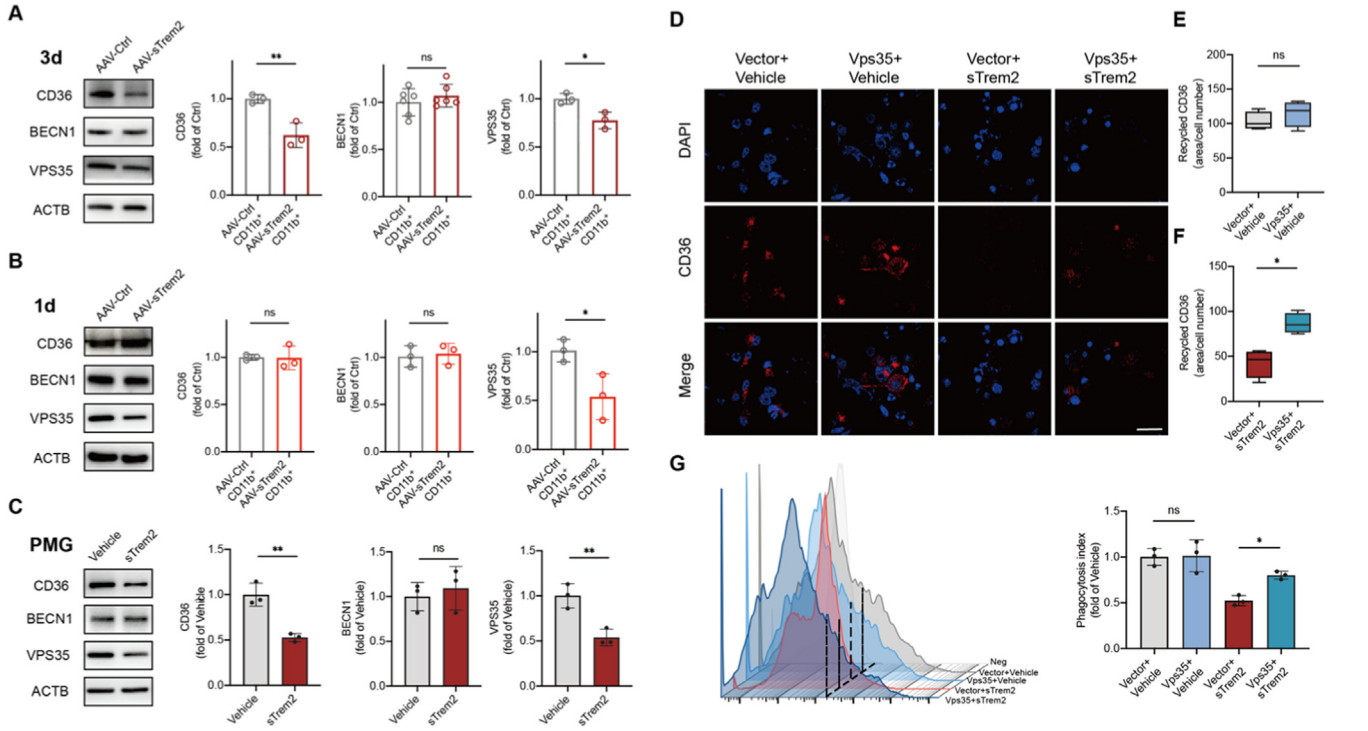

Fig. 6. Vps35 engages in sTrem2-mediated microglial CD36 receptor recycling after ICH. (A) CD36 and receptor recycling associated protein: Beclin1, Vps35 from the CD11b$^+$ cells were analyzed and quantified by Western blotting 3 days after ICH in AAV-Ctrl or AAV-sTrem2 mice. n = 3 per group, $^*p < 0.05$, $^{**}p < 0.01$ versus AAV-Ctrl by Student's *t* test. (B) CD36, Beclin1, and Vps35 from CD11b$^+$ cells from 1 day post-ICH brain tissues. n = 3 per group, $^*p < 0.05$ versus AAV-Ctrl by Student's *t* test. (C) Primary microglia were treated with sTrem2 protein and hemoglobin stimulation. CD36, Beclin1, and Vps35 levels were determined 24 h after treatment. n = 3 per group, $^{**}p < 0.01$ versus Vehicle by Student's *t* test. (D) Representative images of CD36 receptor recycling in BV2 cells transfected with Vps35 or control lentivirus with/without sTrem2 protein administration under hemoglobin stimulation. Scale bar = 50 μm. (E, F) Quantification of recycled receptors in BV2 microglia of each group. n = 3 per group, $^*p < 0.05$ versus Vehicle by Mann–Whitney *U* test. (G) Histogram representing the distribution of RBC-positive BV2 microglia treated with control or Vps35 and vehicle or sTrem2 protein (left). The phagocytic index was analyzed to indicate erythrophagocytosis. n = 3 per group, $^*p < 0.05$ by Student's *t* test.

metabolism under pathological or physiological conditions [33]. The soluble form of Trem2 serves as an immunomodulatory biomarker for Alzheimer's and Parkinson's diseases and ischemic stroke, with few functions yet to be determined [20,49,50]. In a recent study, sTrem2 has been reported to have biological activity in microglial modulation by promoting inflammatory cytokines production and reducing β-amyloid pathology in AD [21,22]. On the other hand, our data suggest that sTrem2 inhibits microglial phagocytosis of RBCs and favors microglia inflammatory phenotype. Moreover, the full-length Trem2 has been shown to accelerate the transformation tworads a neuroprotective and pro-erythrophagocytic microglia cluster that regulates outcomes after ICH; however, sTrem2 significantly impacts the effects on hematoma resolution mediated by full-length Trem2. Thus, the functions of sTrem2 in microglial phagocytosis modulation do not depend on the full-length Trem2 or its related signaling molecular like intracellular adapter DAP12, and there is a bypassing pathway in erythrophagocytosis induced by sTrem2 in ICH.

The observed roles of sTrem2 in RBC engulfment by microglia and macrophages are reminiscent of efferocytosis modification. CD36, a classic scavenger receptor that assists in further hematoma clearance, provides antioxidant protection, and further reduces inflammatory pathway activation [11,31]. SIRP-α, a phagocyte surface receptor of "do not eat me" signaling molecular CD47 protein, is a potential target in ICH [24]. We observed no effects of sTrem2 on the surface expression of SIRP-α (days 1 and 3) and CD36 (day 1) in CD11b + phagocytes, while decreased abundance of CD36 at day 3 post-hemorrhage was observed. Considering that disruption of phagocytic efficiency can be caused by impaired phagocytic receptor recycling [27,28], we showed that sTrem2 interrupts CD36-established receptor recycling method from internalized lysosomes to the plasma membrane. A previous study showed that microglial recycling of CD36 depends on beclin1 and Vps35 [28], and further investigation validated a decrease in Vps35 but not beclin1 in microglia in presence of exocellular abundant sTrem2 after hemorrhagic damage. In Vps35 knock-down microglia, the misrecycled receptor accumulated in the lysosomes and led to an excessive inflammatory response [36]. Our data clearly showed that sTrem2 promoted lysosomal accumulation of CD36, which was then rescued by Vps35 overexpression. However, the interaction between sTrem2 and Vps35 remains unknown, while it was demonstrated that full-length Trem2 directly binds to Vps35 [40]. Based on the knowledge thatTrem2 engages a wide array of molecules and ligands, the potential signal transduction of sTrem2 might also be highly promiscuous, thereby requiring further investigation by high-throughput, multi-omics approaches in future studies.

The Trem2-associated mechanisms of microglia/macrophage phagocytosis in ICH present two aspects: the loss of full-length Trem2, and the sTrem2-induced impairment of CD36 receptor recycling. Several previous studies have focused on pharmacological development. For example, 4D9, a monoclonal antibody has a specific structure "stalk region epitope" which could bind to the cleavage site of Trem2 then stabilize membrane-bound Trem2 and selectively enhance Trem2 associated protective functions in microglia [51]; monoclonal antibody hT2AB promotes Trem2 engagement and basal microglia activation as a surrogate ligand [52]; and monoclonal antibody Ab-T1, which targets Trem2 and changed the ratio of full-length and soluble Trem2 under disease condition [53], improves cognitive function and attenuates chronic neuroinflammation by modulating microglial activation. These biologics provide promising interventions that stabilize

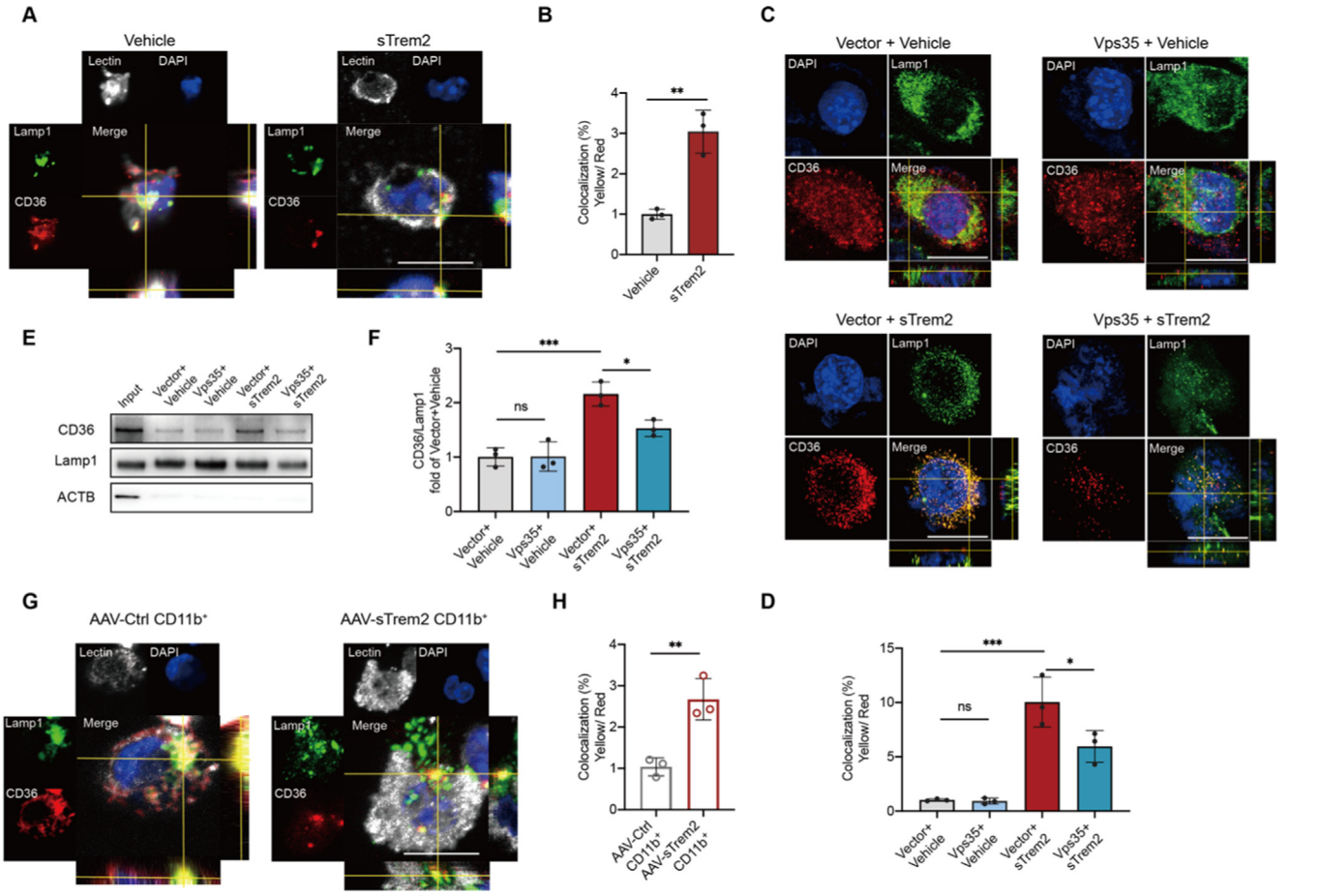

Fig. 7. sTrem2 facilitates lysosomal degradation of unrecycled CD36. (A, B) Representative images and quantification showing colocalization of recycling CD36 (red) and Lamp1 (green) in primary cultured microglia (gray) under sTrem2 administration. Scale bar = 10 μm. n = 3 per group, $^{*}p < 0.05$ versus Vehicle by Student's *t* test. (C, D) Representative images and quantification of CD36 accumulation in BV2 microglial lysosome after control or Vps35 lentivirus infection with/without sTrem2 protein treatment. Scale bar = 10 μm. n = 3 per group. (E, F) BV2 cells were transfected with control or Vps35, and subsequently purified by density gradient centrifugation to obtain lysosome fraction. CD36 accumulated in lysosome of control or Vps35 treated BV2 with/without sTrem2 was analyzed by Western blotting. n = 3 per group, $^{**}p < 0.01$, $^{***}p < 0.001$ versus Vector + Vehicle by one-way ANOVA and Tukey's post hoc test. (G, H) Representative images showing CD36 accumulation in $CD11b^{+}$ cells lysosome from AAV-Ctrl and AAV-sTrem2 infected mice 3 days post ICH. Scale bar = 10 μm, n = 3 per group, $^{*}p < 0.05$ versus AAV-Ctrl by Student's *t* test.

full-length Trem2 hemostasis in the microglial membrane as adjunct therapy for surgical clot removal after ICH, and further experimental evidence is needed for treatment validation.

Although our work provides adequate evidence that sTrem2 impedes microglial erythrophagocytosis and neurological recovery in male mice ICH model, the studies have several limitations. (1) Sex, or estrogen, is an important variable in ICH outcome and microglial functions. Future work to confirm the efficacy of sTrem2 in female ICH mice model is needed. (2) Results were achieved at 3 days and 7 days post ICH induction. Further efforts to discover the effects of a delayed neurological disfunction like altered cognitive function and psychiatric symptoms are cleared needed. (3) Additional studies of the development and discovery of therapeutic strategy to stabilize full-length Trem2 hemostasis in the phagocytes membrane would advance our understanding of the ICH treatment. In conclusion, our results provide strong evidence that sTrem2 is crucially involved in modulating microglial erythrophagocytosis, hindering hematoma clearance and neurological recovery. Our findings shed new light on the roles of sTrem2 in acute brain injury and suggest that rebalancing sTrem2/Trem2 ration may represent a potential target against ICH pathology.

Conclusion

Soluble Trem2 reshapes the microglia/macrophage-mediated erythrophagocytosis through a full-length Trem2 independent mechanism, which impairs the recycling of the pro-erythrophagocytic receptor CD36, thereby impeding hematoma resolution and neurological recovery.

Compliance with ethics requirements

Animal experimentation was approved by the Institutional Animal Ethics Committee of Zhejiang University and performed in accordance with the National Research Council Guide for Care and Use of Laboratory Animals. The ethical approval number for our research is AIRB-2021-607.

Declaration of Competing Interest

The authors declare that they have no known competing financial interests or personal relationships that could have appeared to influence the work reported in this paper.

Acknowledgements

We thank the excellent technical assistance of the Imaging Facility at Zhejiang University School of Medicine and Clinical Research Centre at The Second Affiliated Hospital of Zhejiang University School of Medicine. We also thank Dr. Yuhong Chen for her comments on the manuscript.

Funding

This work was supported by grants from the National Key R&D Program of China (2018YFC1312600, 2018YFC1312603) and the Key Research and Development Project of Zhejiang Province (No. 2018C03011). This study was also supported by the National Natural Science of China (Nos. 81771246, 81971099, 81870908, 82171275, 81901676).

Appendix A. Supplementary material

Supplementary data to this article can be found online at https://doi.org/10.1016/j.jare.2022.03.011.

References

[1] Krishnamurthi RV, Moran AE, Forouzanfar MH, Bennett DA, Mensah GA, Lawes CMM, et al. The global burden of hemorrhagic stroke: a summary of findings from the GBD 2010 study. Glob Heart 2014;9(1):101.
[2] van Asch CJ, Luitse MJ, Rinkel GJ, van der Tweel I, Algra A, Klijn CJ. Incidence, case fatality, and functional outcome of intracerebral haemorrhage over time, according to age, sex, and ethnic origin: a systematic review and meta-analysis. Lancet Neurol 2010;9:167–76. doi: https://doi.org/10.1016/S1474-4422(09)70340-0.
[3] Hankey GJ. Stroke. The Lancet 2017;389:641–54. doi: https://doi.org/10.1016/S0140-6736(16)30962-X.
[4] Krishnamurthi RV, Feigin VL, Forouzanfar MH, Mensah GA, Connor M, Bennett DA, et al. Global and regional burden of first-ever ischaemic and haemorrhagic stroke during 1990–2010: findings from the Global Burden of Disease Study 2010. Lancet Glob Health 2013;1(5):e259–81.
[5] Keep RF, Hua Y, Xi G. Intracerebral haemorrhage: mechanisms of injury and therapeutic targets. Lancet Neurol 2012;11:720–31. doi: https://doi.org/10.1016/S1474-4422(12)70104-7.
[6] Broderick JP, Brott TG, Duldner JE, Tomsick T, Huster G. Volume of intracerebral hemorrhage. A powerful and easy-to-use predictor of 30-day mortality. Stroke 1993;24:987–93. doi: https://doi.org/10.1161/01.str.24.7.987.
[7] Loftspring MC, McDole J, Lu A, Clark JF, Johnson AJ. Intracerebral hemorrhage leads to infiltration of several leukocyte populations with concomitant pathophysiological changes. J Cereb Blood Flow Metab 2009;29:137–43. doi: https://doi.org/10.1038/jcbfm.2008.114.
[8] Mendelow AD, Gregson BA, Fernandes HM, Murray GD, Teasdale GM, Hope DT, et al. Early surgery versus initial conservative treatment in patients with spontaneous supratentorial intracerebral haematomas in the International Surgical Trial in Intracerebral Haemorrhage (STICH): a randomised trial. Lancet 2005;365(9457):387–97.
[9] Hanley DF, Thompson RE, Rosenblum M, Yenokyan G, Lane K, McBee N, et al. Efficacy and safety of minimally invasive surgery with thrombolysis in intracerebral haemorrhage evacuation (MISTIE III): a randomised, controlled, open-label, blinded endpoint phase 3 trial. Lancet 2019;393(10175):1021–32.
[10] Vespa P, Hanley D, Betz J, Hoffer A, Engh J, Carter R, et al. ICES (intraoperative stereotactic computed tomography-guided endoscopic surgery) for brain hemorrhage: a multicenter randomized controlled trial. Stroke 2016;47(11):2749–55.
[11] Zhao X, Sun G, Zhang J, Strong R, Song W, Gonzales N, et al. Hematoma resolution as a target for intracerebral hemorrhage treatment: role for peroxisome proliferator-activated receptor gamma in microglia/macrophages. Ann Neurol 2007;61:352–62. doi: https://doi.org/10.1002/ana.21097.
[12] Lemke G. How macrophages deal with death. Nat Rev Immunol 2019;19:539–49. doi: https://doi.org/10.1038/s41577-019-0167-y.
[13] Taylor RA, Chang C-F, Goods BA, Hammond MD, Mac Grory B, Ai Y, et al. TGF-β1 modulates microglial phenotype and promotes recovery after intracerebral hemorrhage. J Clin Invest 2017;127:280–92. https://doi.org/10.1172/JCI88647.
[14] Chang C-F, Goods BA, Askenase MH, Hammond MD, Renfroe SC, Steinschneider AF, et al. Erythrocyte efferocytosis modulates macrophages towards recovery after intracerebral hemorrhage. Journal of Clinical Investigation 2017;128:607–24. https://doi.org/10.1172/JCI95612.
[15] Wang J, Doré S. Heme oxygenase-1 exacerbates early brain injury after intracerebral haemorrhage. Brain 2007;130:1643–52. doi: https://doi.org/10.1093/brain/awm095.
[16] Schmid CD, Sautkulis LN, Danielson PE, Cooper J, Hasel KW, Hilbush BS, et al. Heterogeneous expression of the triggering receptor expressed on myeloid cells-2 on adult murine microglia. J Neurochem 2002;83(6):1309–20.
[17] Deczkowska A, Weiner A, Amit I. The physiology, pathology, and potential therapeutic applications of the TREM2 signaling pathway. Cell 2020;181:1207–17. doi: https://doi.org/10.1016/j.cell.2020.05.003.
[18] Weber GE, Koenig KA, Khrestian M, Shao Y, Tuason ED, Gramm M, et al. An altered relationship between soluble TREM2 and inflammatory markers in young adults with down syndrome: a preliminary report. JI 2020;204(5):1111–8.
[19] Piccio L, Deming Y, Del-Águila JL, Ghezzi L, Holtzman DM, Fagan AM, et al. Cerebrospinal fluid soluble TREM2 is higher in Alzheimer disease and associated with mutation status. Acta Neuropathol 2016;131(6):925–33.
[20] Suárez-Calvet M, Kleinberger G, Araque Caballero MÁ, Brendel M, Rominger A, Alcolea D, et al. sTREM2 cerebrospinal fluid levels are a potential biomarker for microglia activity in early-stage Alzheimer's disease and associate with neuronal injury markers. EMBO Mol Med 2016;8:466–76. , https://doi.org/10.15252/emmm.201506123.
[21] Zhong Li, Chen X-F, Wang T, Wang Z, Liao C, Wang Z, et al. Soluble TREM2 induces inflammatory responses and enhances microglial survival. J Exp Med 2017;214(3):597–607.
[22] Zhong Li, Xu Y, Zhuo R, Wang T, Wang K, Huang R, et al. Soluble TREM2 ameliorates pathological phenotypes by modulating microglial functions in an Alzheimer's disease model. Nat Commun 2019;10(1). doi: https://doi.org/10.1038/s41467-019-09118-9.
[23] Xu J, Chen Z, Yu F, Liu H, Ma C, Xie Di, et al. IL-4/STAT6 signaling facilitates innate hematoma resolution and neurological recovery after hemorrhagic stroke in mice. Proc Natl Acad Sci U S A 2020;117(51):32679–90.
[24] Jing C, Bian L, Wang M, Keep RF, Xi G, Hua Y. Enhancement of hematoma clearance with CD47 blocking antibody in experimental intracerebral hemorrhage. Stroke 2019;50:1539–47. doi: https://doi.org/10.1161/STROKEAHA.118.024578.
[25] Bennett ML, Bennett FC, Liddelow SA, Ajami B, Zamanian JL, Fernhoff NB, et al. New tools for studying microglia in the mouse and human CNS. PNAS 2016;113(12). doi: https://doi.org/10.1073/pnas.1525528113.
[26] Pluvinage JV, Haney MS, Smith BAH, Sun J, Iram T, Bonanno L, et al. CD22 blockade restores homeostatic microglial phagocytosis in ageing brains. Nature 2019;568(7751):187–92.
[27] Heckmann BL, Teubner BJW, Tummers B, Boada-Romero E, Harris L, Yang M, et al. LC3-associated endocytosis facilitates β-amyloid clearance and mitigates neurodegeneration in murine Alzheimer's disease. Cell 2019;178(3):536–551.e14.
[28] Lucin K, O'Brien C, Bieri G, Czirr E, Mosher K, Abbey R, et al. Microglial beclin 1 regulates retromer trafficking and phagocytosis and is impaired in Alzheimer's disease. Neuron 2013;79(5):873–86.
[29] Zhou H, Hu L, Li J, Ruan Wu, Cao Y, Zhuang J, et al. AXL kinase-mediated astrocytic phagocytosis modulates outcomes of traumatic brain injury. J Neuroinflammation 2021;18(1). doi: https://doi.org/10.1186/s12974-021-02201-3.
[30] Carosi JM, Hattersley KJ, Cui Y, Yang Z, Teasdale RD, Sargeant TJ. Subcellular fractionation of hela cells for lysosome enrichment using a continuous percoll-density gradient. Bio Protoc 2019;9:. , https://doi.org/10.21769/BioProtoc.3362e3362.
[31] Zhuang J, Peng Y, Gu C, Chen H, Lin Z, Zhou H, et al. Wogonin accelerates hematoma clearance and improves neurological outcome via the PPAR-γ pathway after intracerebral hemorrhage. Transl Stroke Res 2021;12(4):660–75.
[32] Hsieh CL, Koike M, Spusta SC, Niemi EC, Yenari M, Nakamura MC, et al. A role for TREM2 ligands in the phagocytosis of apoptotic neuronal cells by microglia. J Neurochem 2009;109:1144–56. doi: https://doi.org/10.1111/j.1471-4159.2009.06042.x.
[33] Kawabori M, Kacimi R, Kauppinen T, Calosing C, Kim JY, Hsieh CL, et al. Triggering receptor expressed on myeloid cells 2 (TREM2) deficiency attenuates phagocytic activities of microglia and exacerbates ischemic damage in experimental stroke. J Neurosci 2015;35(8):3384–96.
[34] Hammond MD, Taylor RA, Mullen MT, Ai Y, Aguila HL, Mack M, et al. CCR2+ Ly6C(hi) inflammatory monocyte recruitment exacerbates acute disability following intracerebral hemorrhage. J Neurosci 2014;34(11):3901–9.
[35] Barclay AN, Van den Berg TK. The interaction between signal regulatory protein alpha (SIRPα) and CD47: structure, function, and therapeutic target. Annu Rev Immunol 2014;32:25–50. doi: https://doi.org/10.1146/annurev-immunol-032713-120142.
[36] Chen D, Xiao H, Zhang K, Wang B, Gao Z, Jian Y, et al. Retromer is required for apoptotic cell clearance by phagocytic receptor recycling. Science 2010;327(5970):1261–4.
[37] Wang W, Wang X, Fujioka H, Hoppel C, Whone AL, Caldwell MA, et al. Parkinson's disease-associated mutant VPS35 causes mitochondrial dysfunction by recycling DLP1 complexes. Nat Med 2016;22(1):54–63.
[38] Bonifacino JS, Hurley JH. Retromer. Curr Opin Cell Biol 2008;20:427–36. doi: https://doi.org/10.1016/j.ceb.2008.03.009.
[39] Temkin P, Lauffer B, Jäger S, Cimermancic P, Krogan NJ, von Zastrow M. SNX27 mediates retromer tubule entry and endosome-to-plasma membrane trafficking of signalling receptors. Nat Cell Biol 2011;13:715–21. doi: https://doi.org/10.1038/ncb2252.
[40] Yin J, Liu X, He Q, Zhou L, Yuan Z, Zhao S. Vps35-dependent recycling of Trem2 regulates microglial function. Traffic 2016;17(12):1286–96.

[41] Yamasaki R, Lu H, Butovsky O, Ohno N, Rietsch AM, Cialic R, et al. Differential roles of microglia and monocytes in the inflamed central nervous system. J Exp Med 2014;211(8):1533–49.
[42] Tong L-S, Shao A-W, Ou Y-b, Guo Z-n, Manaenko A, Dixon BJ, et al. Recombinant Gas6 augments Axl and facilitates immune restoration in an intracerebral hemorrhage mouse model. J Cereb Blood Flow Metab 2017;37 (6):1971–81.
[43] Morioka S, Perry JSA, Raymond MH, Medina CB, Zhu Y, Zhao L, et al. Efferocytosis induces a novel SLC program to promote glucose uptake and lactate release. Nature 2018;563(7733):714–8.
[44] Han CZ, Juncadella IJ, Kinchen JM, Buckley MW, Klibanov AL, Dryden K, et al. Macrophages redirect phagocytosis by non-professional phagocytes and influence inflammation. Nature 2016;539(7630):570–4.
[45] Damisah EC, Rai A, Grutzendler J. TREM2: Modulator of Lipid Metabolism in Microglia. Neuron 2020;105:759–61. doi: https://doi.org/10.1016/j.neuron.2020.02.008.
[46] Nugent AA, Lin K, van Lengerich B, Lianoglou S, Przybyla L, Davis SS, et al. TREM2 regulates microglial cholesterol metabolism upon chronic phagocytic challenge. Neuron 2020;105(5):837–854.e9.
[47] Kim S-M, Mun B-R, Lee S-J, Joh Y, Lee H-Y, Ji K-Y, et al. TREM2 promotes Aβ phagocytosis by upregulating C/EBPα-dependent CD36 expression in microglia. Sci Rep 2017;7(1). doi: https://doi.org/10.1038/s41598-017-11634-x.
[48] Ulland TK, Colonna M. TREM2 — a key player in microglial biology and Alzheimer disease. Nat Rev Neurol 2018;14:667–75. doi: https://doi.org/10.1038/s41582-018-0072-1.
[49] Wilson EN, Swarovski MS, Linortner P, Shahid M, Zuckerman AJ, Wang Q, et al. Soluble TREM2 is elevated in Parkinson's disease subgroups with increased CSF tau. Brain 2020;143:932–43. https://doi.org/10.1093/brain/awaa021.
[50] Kwon HS, Lee E-H, Park H-H, Jin J-H, Choi H, Lee K-Y, et al. Early increment of soluble triggering receptor expressed on myeloid cells 2 in plasma might be a predictor of poor outcome after ischemic stroke. J Clin Neurosci 2020;73:215–8.
[51] Schlepckow K, Monroe KM, Kleinberger G, Cantuti-Castelvetri L, Parhizkar S, Xia D, et al. Enhancing protective microglial activities with a dual function TREM 2 antibody to the stalk region. EMBO Mol Med 2020;12. https://doi.org/10.15252/emmm.201911227.
[52] Ellwanger DC, Wang S, Brioschi S, Shao Z, Green L, Case R, et al. Prior activation state shapes the microglia response to antihuman TREM2 in a mouse model of Alzheimer's disease. PNAS 2021;118(3). doi: https://doi.org/10.1073/pnas.2017742118.
[53] Fassler M, Rappaport MS, Cuño CB, George J. Engagement of TREM2 by a novel monoclonal antibody induces activation of microglia and improves cognitive function in Alzheimer's disease models. J Neuroinflammation 2021;18:19. doi: https://doi.org/10.1186/s12974-020-01980-5.